Electronic Supplementary Information

Reconfigurable all-dielectric Fano metasurfaces for strong full-space intensity modulation of visible light

Sun-Je Kim,[a] Inki Kim,[b] Sungwook Choi,[c] Hyojin Yoon,[d] Changhyun Kim,[a] Yohan Lee,[a] Chulsoo Choi,[a] Junwoo Son,[d] Yong Wook Lee,[c] Junsuk Rho,[b,e] and Byoungho Lee[a]*

a. Inter-University Semiconductor Research Center and School of Electrical and Computer Engineering, Seoul National University, Gwanakro 1, Gwanak-Gu, Seoul 08826, Republic of Korea

b. Department of Mechanical Engineering, Pohang University of Science and Technology (POSTECH), Pohang 37673, Republic of Korea

c. Interdisciplinary Program of Biomedical Mechanical & Electrical Engineering and School of Electrical Engineering, Pukyong National University, Yongso-ro 45, Nam-Gu, Busan 48513, Republic of Korea

d. Department of Materials Science and Engineering, Pohang University of Science and Technology (POSTECH), Pohang 37673, Republic of Korea

e. Department of Chemical Engineering, Pohang University of Science and Technology (POSTECH), Pohang 37673, Republic of Korea

*Corresponding Author‘s E–mail: byoungho@snu.ac.kr

Part 1. Electrical and optical characterization of VO_2 film

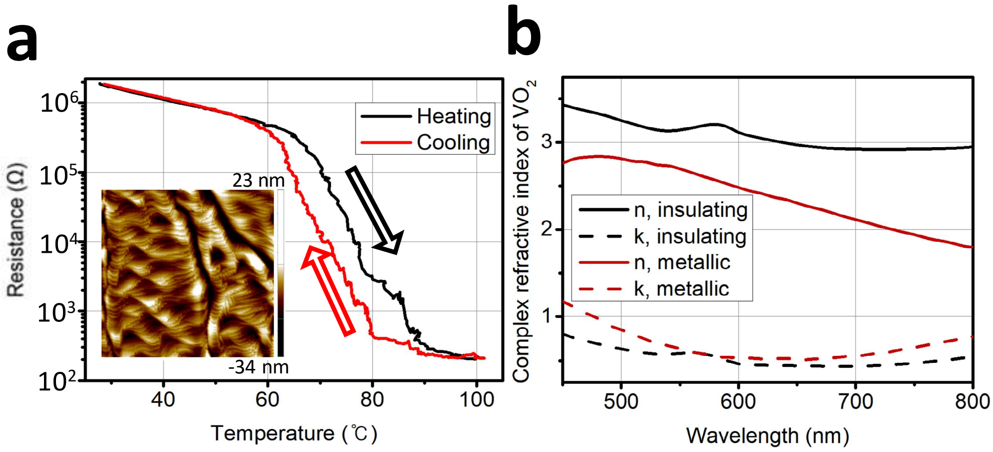

Figure S1. *The temperature-dependent reconfigurable insulator-to-metal transition effect. (a) Measured resistance and (b) refractive index n and extinction coefficient k spectra of VO_2 film. The inset figure of (a) shows surfacial property of 320 nm-thick VO_2 film.*

The electrical resistance and complex dielectric function of VO_2 film grown by pulsed laser deposition are largely tuned in a volatile manner by heating. Resistance and dielectric functions are measured by multi-meter and ellipsometry with additional temperature controllers, respectively. The ellipsometry measurement is conducted at the room temperature and 373 K for uniform and stable saturations of the phase-change of an entire VO_2 thin film.

Part 2. Ellipsometry result of hydrogenated amorphous silicon thin film

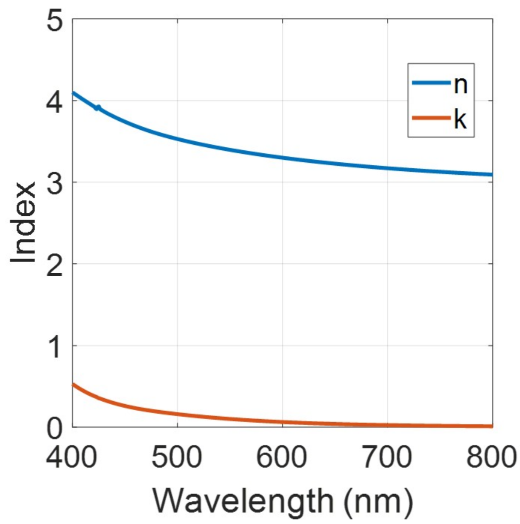

Figure S2. *Measured refractive index (n) and extinction coefficient (k) spectra of hydrogenated amorpohus silicon thin film.*

Part 3. Top view scanning electron micrograph of the VO_2 metafilm and fabrication process

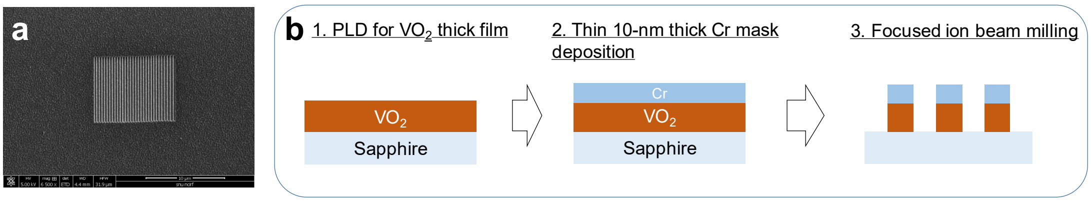

Figure S3. *(a) Top view scanning electron micrograph image of the fabricated VO_2 metafilm with size of 10 µm by 8 µm. (b) Fabrication process of VO_2 metafilm by PLD of VO_2, e-beam evaporation of Cr, and ion beam patterning.*

The fabrication of VO_2 metafilm is conducted via three processes. At first, we used the conventional pulsed laser deposition (LAMBDA PHYSIK,COMPEX 205) system with a KrF excimer laser at 248nm for deposition of a 320nm-thick VO_2 film on the double polished c-cut sapphire substrate. Then, the 10 nm-thick Cr mask, which provides negligible optical effect, is deposited via e-beam evaporation (MUHAN, MHS-1800) to facilitate accurate ion beam milling and prevent gallium ion contamination of the sample during focused ion beam milling. At last, 10 µm by 8 µm sized metafilm pattern is defined by focused ion beam (FEI, Quanta 200 3D) milling.

In case of the HSQ-coated metafilm, we deposited HSQ on the fabricated VO_2 metafilm by the following recipe. We spin-coated HSQ (XR-1541-006, Dow Corning) on the sample at rotation speed of 5000 rpm to demonstrate thickness about 80 nm. Then the sample was post-baked for 4 min at 80 °C.

Part 4. Two port Fano resonance modeling of VO_2 metafilm by temporal coupled mode theory formalism and effective medium theory

Assuming time-dependence of $\exp(i\omega t)$, a single mode resonator with two ports and low total decay rate ($\gamma_{tot} = \gamma_{abs} + \gamma_{rad}$) can be formulated with temporal coupled mode theory[1-5] as the following equations (S1)-(S3).

$$\frac{du}{dt} = (i\omega_0 - \gamma_{abs} - \gamma_{rad})u + d_1 s_{1+}, \tag{S1}$$

$$s_{1-} = r_d s_{1+} + d_1 u,\ s_{2-} = t_d s_{1+} + d_2 u, \tag{S2}$$

$$|d_1|^2 + |d_2|^2 \approx 2\gamma_{rad}. \tag{S3}$$

Here, u, ω_0, γ_{abs}, γ_{rad}, and d_i refer to complex amplitude of resonator mode, angular frequency of a resonance, internal loss-induced decay rate, external radiative decay rate, and coupling coefficient between a resonator and normal radiation mode (s_{1+}), respectively, while $|u|^2 = W$ is equal to the energy in the resonator. Equations (S2) and (S3) reveal the time-reversal property and energy conservation law assuming single port system approximation, respectively. As mentioned in the manuscript, total reflection (r_{tot}) and total transmission (t_{tot}) can be modelled as a sum of direct and indirect pathways. Here, r_d and t_d can be theoretically calculated with Airy's formula of infinite series while $n_{eff} = \sqrt{\varepsilon_{vo2} f_{vo2} + \varepsilon_{air}(1 - f_{vo2})}$ for TE illumination and $n_{eff} = \sqrt{\left\{\varepsilon_{vo2}^{-1} f_{vo2} + \varepsilon_{air}^{-1}(1 - f_{vo2})\right\}^{-1}}$ for TM illumination, respectively. k_0 and t denote free space wavenumber and thickness of a metafilm, respectively. Resultantly, r_{tot} and t_{tot} can be approximately formulated as the equations (S4 and S5) below. a and b are a positive-valued constant.

$$r_{tot} = \frac{s_{1-}}{s_{1+}} \approx r_d + \frac{d_1^{\,2}}{i(\omega - \omega_0) + (\gamma_{abs} + \gamma_{rad})} \approx r_d + \frac{ae^{i\rho}}{i(\omega - \omega_0) + \gamma_{tot}}. \tag{S4}$$

$$t_{tot} = \frac{s_{2-}}{s_{1+}} \approx t_d + \frac{d_1 d_2}{i(\omega - \omega_0) + (\gamma_{abs} + \gamma_{rad})} \approx t_d + \frac{be^{i\varphi}}{i(\omega - \omega_0) + \gamma_{tot}}. \tag{S5}$$

Part 5. Lorentzian fitting of indirect reflectance in VO_2 metafilm at the insulating phase

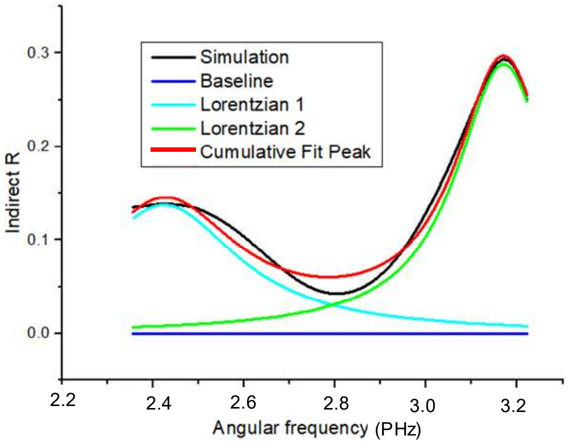

Figure S4. *Lorentzian fitting results of indirect reflectance with dual resonances.*

The fitting of dual resonant indirect reflectance and transmittance are fitted by approximated local single Lorentzian resonance modelling and fitting according to the equation below and fitting parameters are suggested in the two tables below.

$$I = \frac{(A_1\gamma_1/\pi)}{(\omega-\omega_{0,1})^2+\gamma_1^2}+\frac{(A_2\gamma_2/\pi)}{(\omega-\omega_{0,2})^2+\gamma_2^2}. \qquad \text{(S6)}$$

Table S1. *Fitting parameters of insulating phase indirect reflectance of VO_2 metafilm.*

	Value (peak 1)	Value (peak 2)
ω_0	2.42438E15	3.17E15
γ	1.978545E14	1.28079E14
A	8.53661E13	1.1593E14

Part 6. Numerical simulation results of the non-tapered VO_2 metafilm

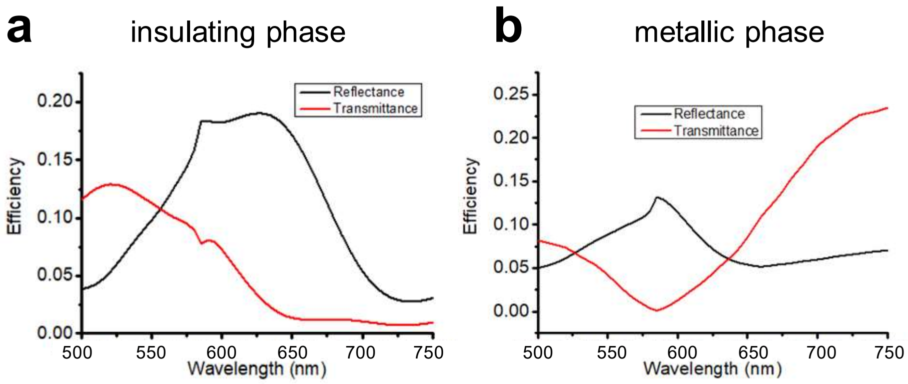

Figure S5. *Simulation results of the non-tapered metafilm reflectance (the zeroth order) and transmittance (the zeroth order) at the (a) insulating and (b) metallic phases, respectively.*

Part 7. Approximated optical description of intermediate VO_2 phase by using Maxwell-Garnett effective medium theory

For numerical estimation of the continuous modulation capability utilizing intermediate phases, Maxwell-Garnett effective medium theory is used to express intermediate VO_2 phase where the insulating and metallic phases coexist. When filling factor of metallic VO_2, *f,* varies from 0 to 0.4, host material is set to be the insulating VO_2. Thus, effective dielectric function of VO_2 in this range is expressed as $\varepsilon_{eff}(f) = \varepsilon_i[\varepsilon_m(1+2f)+\varepsilon_i(2-2f)]/[\varepsilon_m(1-f)+\varepsilon_i(2+f)]$. On the other hand, when *f* varies from 0.6 to 1, host material is set to be the metallic VO_2 and effective dielectric function of VO_2 region is set to be $\varepsilon_{eff}(f) = \varepsilon_m[\varepsilon_m \cdot 2f + \varepsilon_i(3-2f)]/[\varepsilon_m(3-f)+\varepsilon_i \cdot f]$.

Part 8. VO_2 metafilm measurements in cooling process and modulation depth

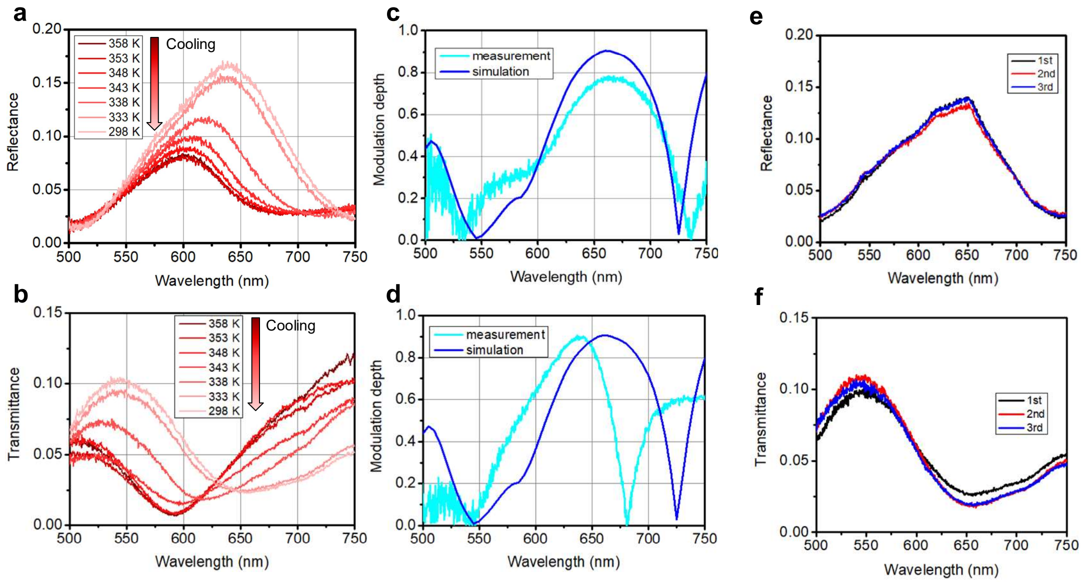

Figure S6. Measurement result of VO_2 metafilm in cooling process of (a) reflectance and (b) transmittance. Modulation depth of (c) reflectance and (d) transmittance from simulation and measurement results. Repetitive cyclic measurement results of (e) reflectance and (f) transmittance at the room temperature to check measurement stable reconfigurability.

Part 9. Lorentzian fitting of indirect scatterings of HSQ coated VO_2 metafilm at the insulating phase

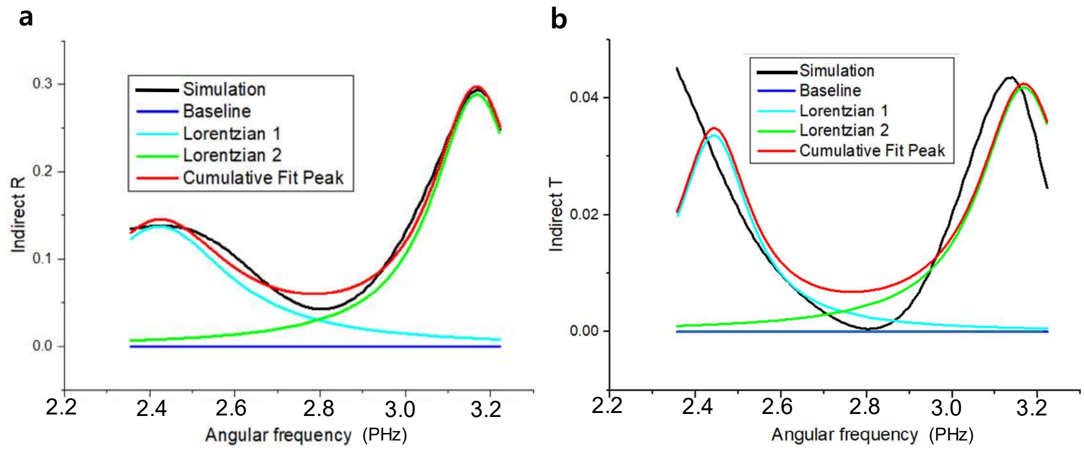

Figure S7. Lorentzian fitting results of indirect (a) reflectance and (b) transmittance with dual resonances.

The fitting of dual resonant indirect reflectance and transmittance are fitted by approximated local single Lorentzian resonance modelling and fitting according to the Equation (S6) and fitting parameters are suggested in the two tables below.

Table S2. *Fitting parameters of insulating phase indirect reflectance of HSQ-coated VO_2 metafilm.*

Reflection	Value (Peak 1)	Value (Peak 2)
ω_0	2.42282E15	3.1679E15
γ	1.988015E14	1.27252E14
A	8.58069E13	1.15194E14

Table S3. *Fitting parameters of insulating phase indirect transmittance of HSQ-coated VO_2 metafilm.*

Transmission	Value (Peak 1)	Value (Peak 2)
ω_0	2.42282E15	3.1679E15
γ	1.01723E14	1.27252E14
A	1.07321E13	1.67004E13

Part 10. The HSQ coated VO_2 metafilm measurements in cooling process and modulation depth

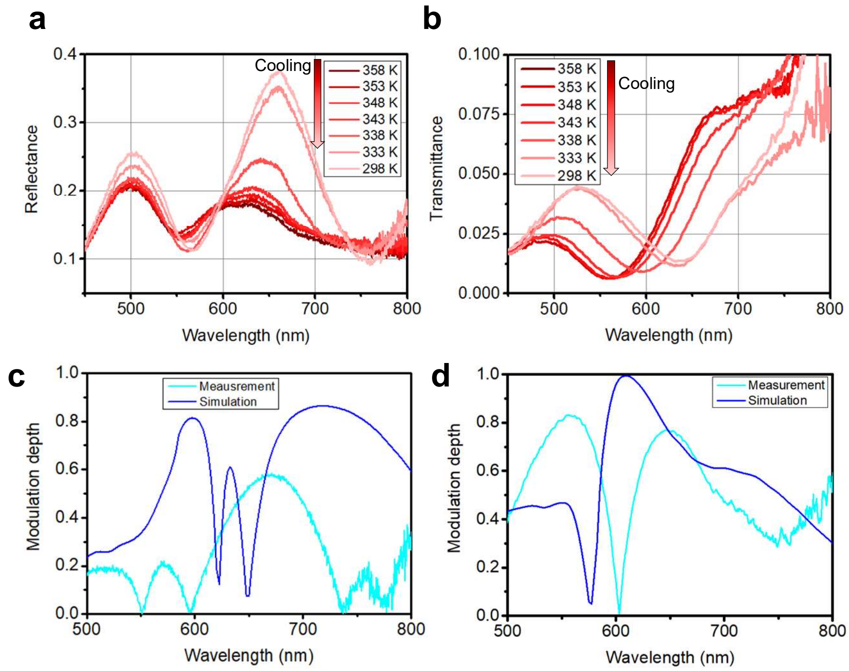

Figure S8. *Measurement result of HSQ coated VO_2 metafilm in cooling process of (a) reflectance and (b) transmittance. Modulation depth of (c) reflectance and (d) transmittance from simulation and measurement results.*

Part 11. The effect of oblique incidence on the zeroth order reflectance and transmittance spectra of the HSQ-coated metafilm

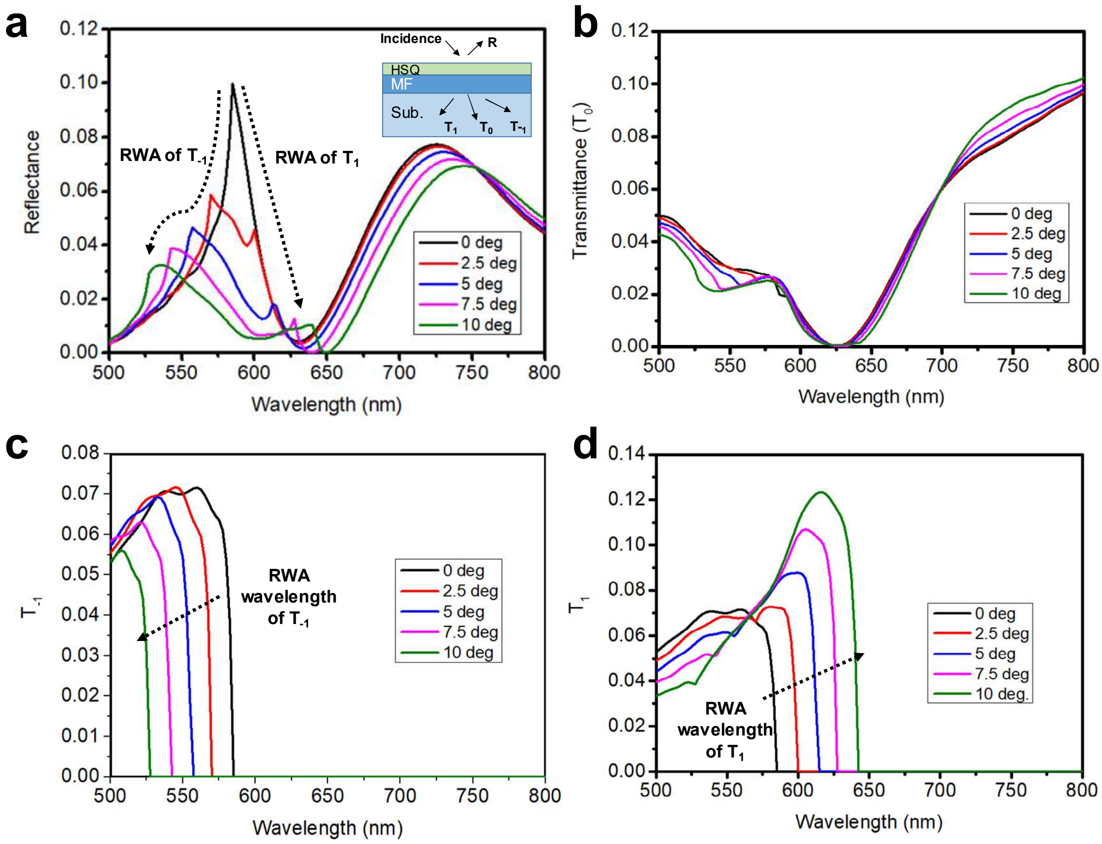

Figure S9. *Effect of oblique incidence angle on (a) reflectance, (b) the 0th order transmittance (T_0), (c) the -1st order diffractive transmittance (T_{-1}), and (d) the 1st order diffractive transmittance (T_1) of the HSQ-coated VO_2 metafilm calculated by numerical simulations at the insulating phase. The inset figure of (a) conceptually describes the oblique illumination circumstance with asymmetric diffractive transmission channels. The legends in (a)-(d) denote incidence angle of TM polarized light.*

For thorough analysis of the difference near RWA resonance between the simulation and measurement results presented in the manuscript Figure 3, we conducted additional simulations for various oblique TM incidences. According to the numerical simulations presented in Figures S9, the presence of portion of oblique illumination of light in experiment significantly change the position and strength of the sharp RWA reflectance peak (Fig. S9(a)) in the HSQ-coated VO_2 metafilm rather than the 0th order transmittance shown in Fig. S9(b). Such change originates from change of phase-matching condition according to varying incidence angle. As the incidence angle increases, the position of RWA resonance at the normal illumination case ($\lambda_{RWA} = pn_{sub}$) splits to the blue shifted -1st order at $\lambda_{RWA} = pn_{sub}(1-\sin\theta_i)$ and the red shifted 1st order at $\lambda_{RWA} = pn_{sub}(1+\sin\theta_i)$ as described in plot of Fig. S9(c) and (d), respectively.

It seems that the sensitivity of RWA condition according to slightly oblique incidence might be the main reason since the sharp RWA of reflectance is not measured and the blue shifted moderate resonance is measured (Fig. 3(f)), while the 0th order transmittance is not much affected by oblique illumination (Fig. 3(h), Fig. S9(b)).

Part 12. Microspectroscopy setup

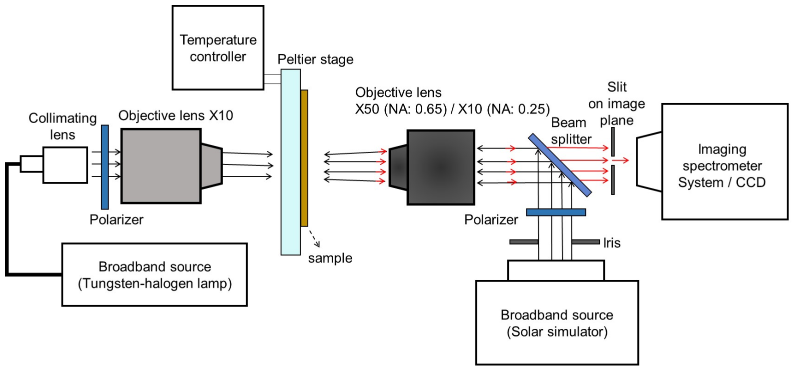

Figure S10. *Schematic diagram of micro-spectroscopy setup for measurement of temperature-controlled reflection and transmission spectra.*

Part 13. Ellipsometry result of VO_2 thin film (50 nm thick film deposited by sputtering)

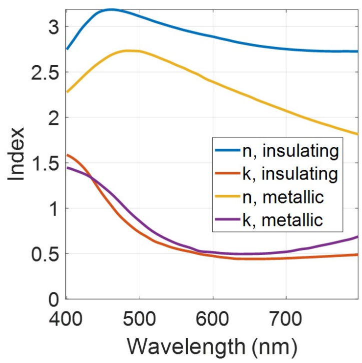

Figure S11. *Measured refractive index (n) and extinction coefficient (k) spectra of sputtered 50 nm-thick VO_2 thin film at the insulating (room temperature) and metallic (373 K) phases.*

Part 14. Fabrication process of hybrid metagrating device

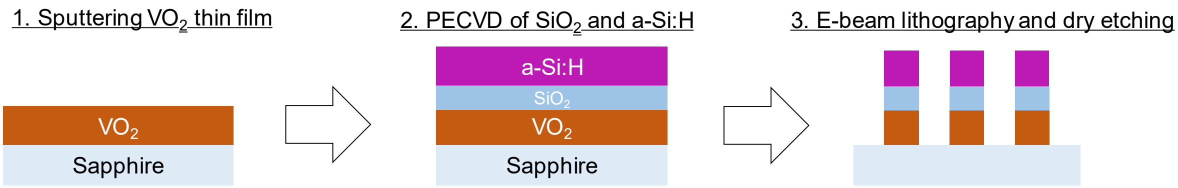

Figure S12. *Fabrication process of hybrid metagrating.*

The fabrication of the hybrid metagrating device that consists of VO_2, SiO_2 and a-Si:H starts from preparation of c-cut sapphire substrate. A 50 nm-thick VO_2 thin film is deposited by using a vanadium sputtering process followed by corresponding oxidation process to realize VO_2 phase state. Onto the film, a 10 nm-thick SiO_2 and a 80 nm-thick a-Si:H film are deposited by using a plasma enhanced chemical vapor deposition. On this multilayer-coated substrate, the nanograting patterns are transferred in the polymethyl methacrylate (PMMA) (Microchem, 495 PMMA A2) by using a standard electron beam lithography (EBL) process with 80 kV-acceleration voltage and 50 pA beam current. The PMMA layer is spin-coated on the substrate with 2,000 rpm for 60 sec, and following conductive polymer is spin-coated on the substrate with 2,000 rpm for 60 sec to prevent charging effect from dielectric substrate. After EBL exposure step, the conductive polymer is removed by de-ionized water and PMMA layer is developed in the MIBK:IPA 1:3 solutions for 12 mins. Then, 30 nm-thick chromium (Cr) is deposited by using an electron beam evaporator followed by lift-off process. Using a dry etching process with Cl_2 gas and HBr gas, Cr nanograting patterns are transferred to multilayer structure.

Part 15. Fano resonance fitting results of the RWA reflectance in the hybrid metagrating

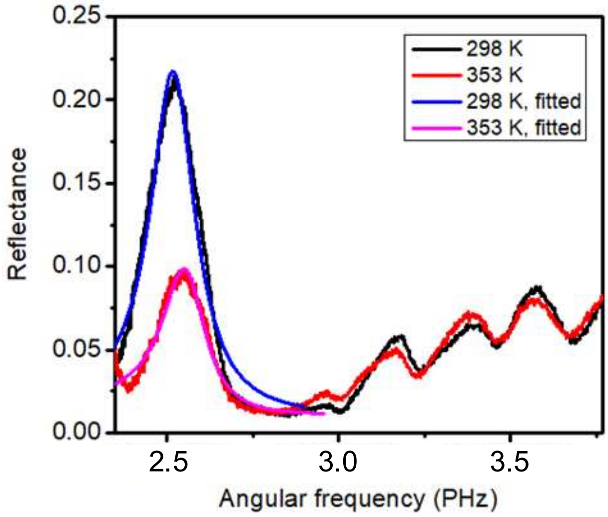

Figure S13. *Reflectance spectra of measurement and Fano resonance fitting near the RWA peaks of them at the insulating (298 K) and metallic phases (353 K) of VO_2, respectively.*

The RWA reflectance results from both the simulation (Fig. 4(c)) and measurement (Fig. S14) are fitted as Fano resonance according to the equation below and the detailed fitting parameters are suggested in the table S4.

$$R = R_0 + \frac{H\left(\frac{(\omega-\omega_0)}{q}+\gamma\right)^2}{(\omega-\omega_0)^2+\gamma^2}.$$

Table S4. *Fano resonance fitting parameters of the simulation and measurement results of the hybrid metagrating*

	Value (insulating phase, simulation)	Value (insulating phase, measurement)	Value (metallic phase, simulation)	Value (metallic phase, measurement)
R_0	0.24545	0.00968	0.02359	0.01104
ω_0	2.66226E15 Hz	2.52045E15 Hz	2.66425E15 Hz	2.55949E15 Hz
H	0.25063	0.20751	0.06245	0.08606
γ	6.03371E13	7.9291E13	1.17485E14	7.70566E13
q	-26.5929	-27.19128	-14.1702	-8.19846

Part 16. Transmittance and measurements of hybrid metagrating device in cooling process

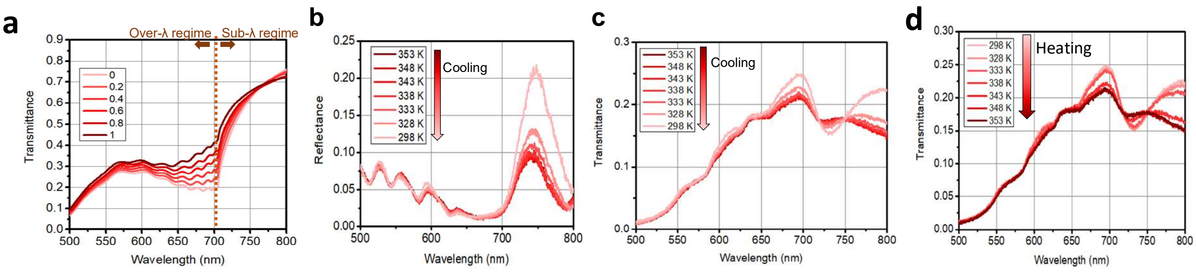

__Figure S14.__ (a) Numerical simulation results of gradually tunable transmittance near RWA resonance. The inset denotes filling factor of metallic VO_2. Measurement result of hybrid metagrating in cooling process of (b) reflectance and (c) transmittance. (d) Transmittance change in heating process.

Part 17. Effect of oblique incidence in RWA resonance in the hybrid metagrating

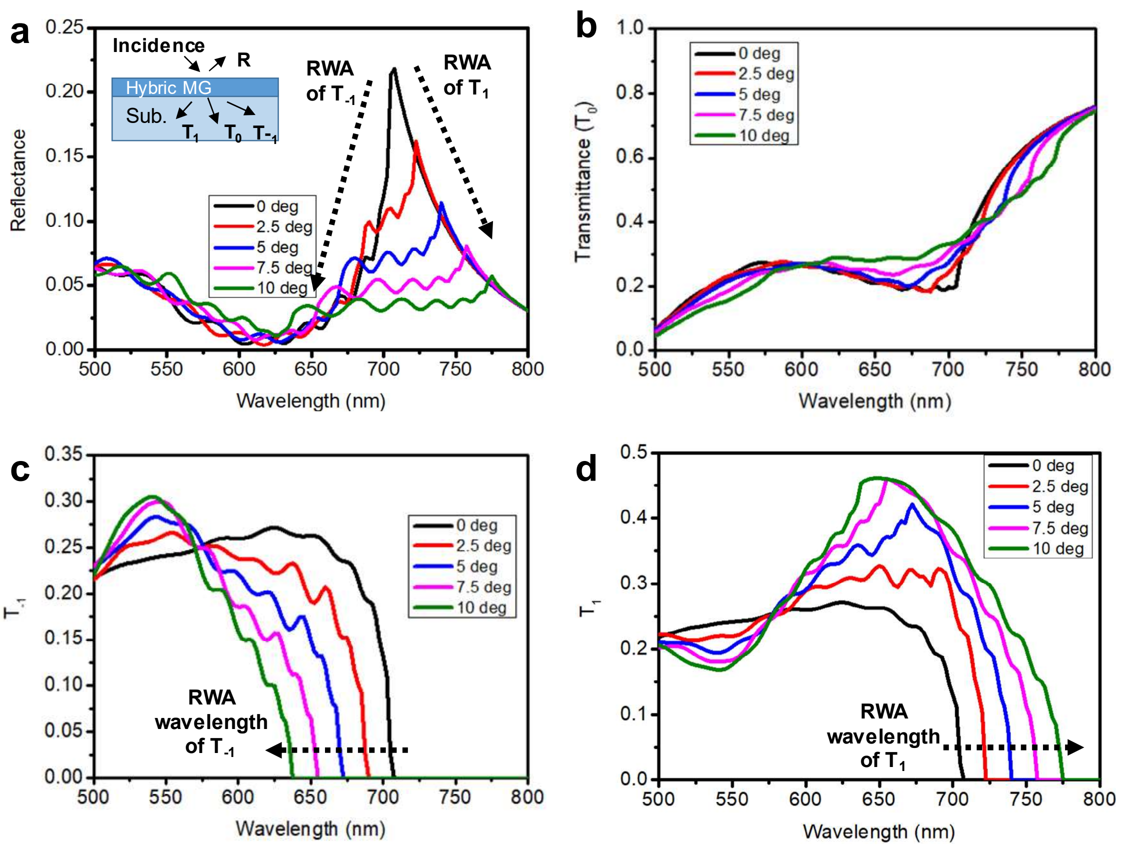

__Figure S15.__ Effect of oblique incidence angle on (a) reflectance, (b) the 0th order transmittance (T_0), (c) the -1st order diffractive transmittance (T_{-1}), and (d) the 1st order diffractive transmittance (T_1) of the hybrid VO_2 metagrating calculated by numerical simulations at the insulating phase. The inset figure of (a) conceptually describes the oblique illumination circumstance with asymmetric diffractive transmission channels. The legends in (a)-(d) denote incidence angle of TM polarized light.

Similar to the analysis of the HSQ-coated VO_2 metafilm suggested in Part 11, for analyzing the difference near RWA resonance between the simulation and measurement results presented in the manuscript Figure 4, we conducted additional simulations for various oblique TM incidences of the VO_2 metagrating device. According to the numerical simulation results presented in Figure S15, the presence of portion of oblique illumination of light in experiment mainly induces the redshift and broadening of the sharp RWA resonance ((Fig. S15(a) and (b))), particularly, for reflectance. Similar to the case of the HSQ-coated VO_2 metafilm studied in Part 11, the degenerate RWA reflectance peak for normal illumination ($\lambda_{RWA} = pn_{sub}$) splits (Fig. S15(a)) to the blue shifted -1st order at $\lambda_{RWA} = pn_{sub}(1-\sin\theta_i)$ and the red shifted 1st order at $\lambda_{RWA} = pn_{sub}(1+\sin\theta_i)$ as described in plot of Fig. S15(c) and (d), respectively. Hence, it seems that the sensitivity of RWA condition according to slightly oblique incidence might be the main reason of slight broadening and redshift (~40 nm) of the RWA reflectance peak shown in the measurement (Fig. 4(f)).

Moreover, we guess that the RWA peak of the hybrid metagrating was detected with better quality rather than that of the HSQ-coated VO_2 metafilm, owing to larger sample size (50 μm by 50 μm) and use of lower numerical aperture objective lens (NA: 0.25, 10X) (See the measurement setup in Part 12.).

References (also cited in the manuscript)

1. H. A. Haus, *Waves and Fields in Optoelectronics*, Prentice-Hall, 1984.
2. S. Fan, W. Suh, and J. D. Joannopoulos, *J. Opt. Soc. Am. A*, 2003, **20**, 569-572.
3. A. Cordaro, J. V. D. Groep, S. Raza, E. F. Pecora, F. Priolo, and M. L. Brongersma, *ACS Photonics*, 2019, **6**, 453-459.
4. J. W. Yoon and R. Magnusson, *Opt. Express*, 2013, **21**, 17751-17759.
5. J. Park, J. H. Kang, S. J. Kim, X. Liu, and M. L. Brongersma, *Nano Lett.*, 2017, **17**, 407-413.